Research Article

# Highly efficient removal of As(V) using metal–organic framework BUC-17

Da Pang[1] · Peng Wang[1] · Huifen Fu[1] · Chen Zhao[1] · Chong-Chen Wang[1]

Received: 23 September 2019 / Accepted: 6 January 2020 / Published online: 10 January 2020


**Abstract**
Arsenic contamination is a great threat worldwide due to its toxicity and hardly degradable. The development of highly efficient adsorbents is an essential challenge in the water treatment field. A 2D metal–organic framework $[Co_3(tib)_2(H_2O)_{12}](SO_4)_3$ (**BUC-17**) has been synthesized by hydrothermal method, and was utilized as an efficient adsorbent to remove As(V) from contaminated water. The results showed that **BUC-17** have higher adsorption capacity toward As(V) than most counterpart adsorbents, its maximum uptake capacity reached 129.2 mg $g^{-1}$ at 298 K. The adsorption kinetics and isotherm behaviors were well fitted with pseudo-second-order and Langmuir model, respectively. The thermodynamic parameters such as free energy change ΔG°, enthalpy change ΔH° and entropy change ΔS° were both negative during the sorption process, suggesting that the adsorption process of **BUC-17** towards As(V) was spontaneous and exothermal. The influence of pH and foreign ions on the adsorptive removal of As(V) using **BUC-17** were investigated. The results showed that pH values have significant influence while co-existed anions (unless phosphate) exert slight effect on adsorption capacity. Finally, a corresponding adsorption mechanism was proposed and confirmed by scanning electron microscopy, Fourier Transform infrared spectra (FTIR) and X-ray photoelectron spectroscopy analysis.

**Keywords** BUC-17 · Arsenic · Adsorption · Mechanism · Performance

## 1 Introduction

Arsenic is extensively distributed in the biosphere and has been linked with toxic and carcinogenic effects [1]. The chronical exposure to arsenic leads to nausea, cancer, muscular weakness, neurological disorder, appetite weakness and impairments of the immune system [2–5]. Most arsenic compounds in the environment are discharged from coal combustion, production of industrial raw materials, arsenic pesticides, or volcano eruption [6, 7]. As a result of their strong toxicity and widely distribution, over 140 million people all over the world, especially in India, Bangladesh, Argentina, Vietnam and China, are facing the tremendous threat of arsenic [8–10]. The World Health Organization has regarded arsenic as a human carcinogen in drinking water and set a provisional standard of no more than 10 μg $L^{-1}$ [11]. In natural waterbody, the arsenic exists in both inorganic arsenic compounds like arsenate, arsenite, and organic arsenic compounds like ASA (Arsanilic, $C_6H_8AsNO_3$) and ROX (Roxarsone, $C_6H_6AsNO_6$), in which As(V) is the primary arsenic species [12]. The existence of inorganic arsenic in natural water depends on the redox conditions. For example, As(V) will be converted into As(III) in the presence of reductive substances [13]. As well, it was well-recognized that the pre-oxidation of As(III) into As(V) is a necessary step for the efficiency of arsenic removal [14, 15]. Inorganic arsenic can be methylated in human body, which leads to the transformation from As(V) to

✉ Chong-Chen Wang, chongchenwang@126.com | [1]Beijing Key Laboratory of Functional Materials for Building Structure and Environment Remediation/Beijing Advanced Innovation Centre for Future Urban Design, Beijing University of Civil Engineering and Architecture, Beijing 100044, China.

As(III), resulting in a great potential threat to human health and environment [1, 16, 17]. Therefore, it is important to remove As(V) from polluted water.

Up to now, there are various techniques for arsenic removal like chemical precipitation, ion exchange, membrane filtration, biological processes and adsorption [3, 18–20], in which the adsorption is widely used in wastewater decontamination due to the advantages such as low cost, high speed, high efficiency and easy operation [21–23]. Traditional adsorbents including activated carbon [24], hydrotalcite [25], red mud [26] and activated alumina [27] are facing problems like low adsorption capacity. It was urgent and essential to develop new adsorbent materials with high efficiency to eliminate arsenic in wastewater.

Metal–organic frameworks (MOFs) are unique porous crystalline materials with large surface area, abundant binding site, regular channel, and tunable morphology, which are widely used in the fields of photocatalysis, adsorption, gas storage and separation [28–32]. Adsorptive removal of arsenic using MOFs have attracted extensive attentions due to their outstanding adsorption capacity, high removal efficiency, short reaction time and wide range of suitable pH values [7, 12, 33, 34]. Furthermore, MOFs possess abundant metal sites even unsaturated coordination sites, which can be coordinated with arsenic for enhanced adsorption ability [35, 36]. However, many MOFs are not stable in water, which exerted great difficulty to carry out reuse and recyclability [37].

A new 2D metal–organic framework $[Co_3(tib)_2(H_2O)_{12}](SO_4)_3$ (**BUC-17**) has been synthesized from tib (1,3,5-tris(1-imidazolyl)benzene) and $Co^{2+}$ by hydrothermal methods, which exhibited ultrahigh adsorption capacity towards some organic dyes [38] as well as Cr(VI) [39]. Considering that **BUC-17** displayed preferential uptake to anionic matters, it was used to carry out adsorptive removal toward As(V) in $HAsNa_2O_4$. Also, the corresponding kinetics, isotherms and the thermodynamic parameters were fitted and calculated. Finally, the adsorption mechanism between **BUC-17** and As(V) was proposed, and confirmed by scanning electron microscopy (SEM), Fourier Transform infrared spectra (FTIR) and X-ray photoelectron spectra (XPS) analyses.

## 2 Materials and methods

### 2.1 Synthesis of BUC-17

All the chemicals were reagent grade and used without further purification. **BUC-17** was synthesized following the reported method [38, 39] with minor modification. Briefly, $CoSO_4{\cdot}7H_2O$ (0.3 mmol, 0.0843 g) and 1,3,5-tris(1-imidazolyl)benzene (tib) (0.3 mmol, 0.0828 g) were mixed with 10 mL deionized water and then added 5 mL ethanol (99%) in a 25 mL Teflon-lined stainless steel Parr bomb, and heated in a drying oven at 413 K for 72 h. The pink powders are acquired by filtration, and then washed three times using deionized water and ethanol (99%) in turn to obtain pure **BUC-17**.

### 2.2 Characterization

The Fourier transform infrared (FTIR) spectra were used to analyze the change of adsorbent throughout the whole adsorption process by a Nicolet 6700 FTIR spectrometer with KBr pellets in the range of 4000–400 $cm^{-1}$. The morphologies and the elemental mappings for adsorbent BUC-17 before and after adsorption were acquired on a FEI Quanta 250 FEG scanning electron microscope (SEM) equipped with Bruker XFlash 5010 Energy Dispersive Spectrometer (EDS). The change of crystalline structures and compositions of the before and after adsorbed samples were characterized by powder X-ray diffraction (PXRD) under Cu K$\alpha$ radiation in the $2\theta$ range of 5°–50° on Dandonghaoyuan DX-2700B diffractometer. X-ray photoelectron spectra (XPS) measurement was carried out on Thermo ESCALAB 250XI to determine adsorbent with its chemical valence state and composition.

### 2.3 Adsorption experiments

An aqueous stock solution of As(V) (500 mg $L^{-1}$) was prepared by dissolving $HAsNa_2O_4{\cdot}7H_2O$ (SIGMA, 98%, 0.5206 g) in deionized water (250 mL), and then stored in the dark at 277 K. The pH values of As(V) solution were adjusted by using aqueous NaOH (0.1 M) or HCl (0.1 M) solution. 40 mg **BUC-17** samples were added to 200 mL of As(V) solution with initial concentrations of 5 mg $L^{-1}$ to 100 mg $L^{-1}$. The mixtures were placed on the constant temperature shaker under speed of 170 r $min^{-1}$ at 298 K, 303 K, 308 K. During the shaking process, 5 mL samples were drawn from the suspensions and then separated by a 0.22 μm membrane filter for further analysis. The residual As(V) concentration was analyzed by ICP-OES (ICP-5000, Focused Photonics (Hangzhou) Inc). The adsorption capacity q (mg $g^{-1}$) was obtained by Eq. (1):

$$q = (C_0 - C_e)V/m \quad (1)$$

where, $C_0$ and $C_e$ are the initial and equilibrium concentrations (mg $L^{-1}$) of As(V), respectively; V is the solution volume (L) and $m$ is the dosage of the adsorbent (g).

## 3 Results and discussion

### 3.1 Adsorption kinetics

In order to determine the effect of contact time on adsorption process of As(V) by **BUC-17**, it was necessary to conduct series of experiments to study the adsorption kinetics. 40 mg **BUC-17** samples were added to 200 mL As(V) solution with initial concentrations ranging from 5 mg $L^{-1}$ to 100 mg $L^{-1}$ (pH = 10) at 298 K for 48 h. The relationships between adsorption capacity and constant time are given in Fig. 1. The maximum adsorption capacity of **BUC-17** toward AS(V) was 129.2 mg $g^{-1}$, which was higher than those of counterpart adsorbents like MIL-53(Al) [18], ZIF-8 [37] and other MOFs as listed in Table 1. For the initial As(V) concentrations of 50 and 100 mg $L^{-1}$, 90% equilibrium adsorption capacities were achieved within first 3 h, and the adsorption equilibrium was accomplished for As(V) solution with concentration of 50 and 100 mg $L^{-1}$within 12 h. To analyze adsorption kinetics and describe the adsorption behaviors, the pseudo first-order [27] and pseudo second-order kinetic [12, 40] models (Eqs. (2) and (3)) were fitted to the kinetic data.

$$\ln(q_e - q_t) = \ln(q_e) - K_1 t \quad (2)$$

$$t/q_t = 1/(K_2 q_e^2) + t/q_e \quad (3)$$

where, $q_e$ and $q_t$ (mg $g^{-1}$) are the adsorption quantities of As(V) at equilibrium time and at a sometime t, respectively. $K_1$ ($min^{-1}$) and $K_2$ (g $mg^{-1}$ $min^{-1}$) are the adsorption rate constants of the pseudo first-order and the pseudo-second-order adsorption, respectively.

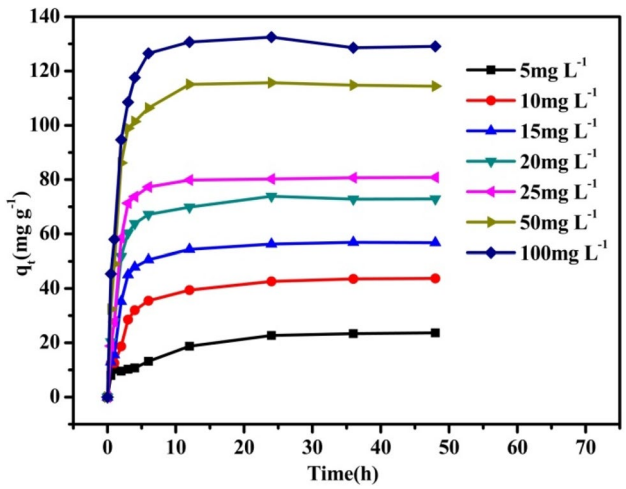


**Fig. 1** The adsorption capacities of **BUC-17** toward As(V) with different initial concentrations (pH = 10.0, $T$ = 298 K)

**Table 1** The adsorption capacities of different adsorbents toward As(V)

| Adsorbents | Adsorption capacity (mg $g^{-1}$) | Equilibrium time | References |
|---|---|---|---|
| ZIF-8 | 106.7 | 24 h | [37] |
| ZIF-8 nanoparticles | 60.03 | 24 h | [36] |
| Hierarchical ZIF-8 | 90.92 | NA | [41] |
| MIL-53(Al) | 105.6 | 48 h | [18] |
| MIL-53(Fe) | 21.27 | NA | [42] |
| UIO-66 | 68.21 | 20 min | [34] |
| UiO-66($NH_2$) | 71.13 | NA | [34] |
| MIL-88A microrods | 145 | 12 h | [12] |
| RT-Zn-MOF-74 | 99 | NA | [43] |
| HT-Zn-MOF-74 | 48.7 | NA | [43] |
| $NH_2$-MIL-88(Fe) | 125 | NA | [33] |
| MOF-808 nanoparticles | 24.83 | NA | [44] |
| $CoFe_2O_4$@MIL-100(Fe) | 114.8 | 24 h | [45] |
| **BUC-17** | 129.2 | 12 h | This work |

From Fig. 2 and Table 2, it can be observed that the adsorption process were better fitted in the pseudo-second-order kinetic models, owing to higher correlation coefficient and narrow difference between the experimental and theoretical values of equilibrium adsorption capacity. It indicated that the rate-limiting step might be chemisorption [7]. Furthermore, to investigate the effect of intraparticle diffusion and ensure the rate limiting step, the Weber–Morris model [46] as represented by Eq. (4) was used to process the kinetics data.

$$q_t = Kt^{1/2} + C \quad (4)$$

where, K (mg $g^{-1}$ $min^{-1/2}$) is the intraparticle diffusion rate constant. The adsorption process could be mainly divided into two sub-processes as shown in Fig. 3. Firstly, the part of steeper slope with faster adsorption rate corresponds to external transfer step, in which the As(V) is adsorbed onto the external surface of **BUC-17**. Secondly, the adsorbed As(V) is further spread from the surface to the internal active sites of **BUC-17** until the adsorption equilibrium is reached, which corresponds to the intraparticle diffusion and equilibrium step. The second step is generally slow evidenced by small adsorption rate [12]. It is worthy to note that the higher initial As(V) concentration results into the faster adsorption rate of external transfer step (first step), due to the fact that the higher initial concentrations can enhance diffusion driving force [12, 36].

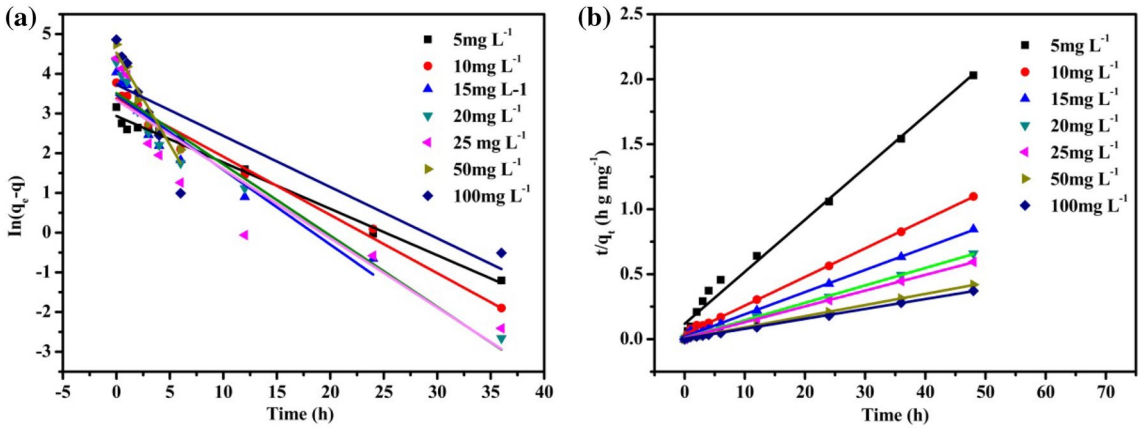


**Fig. 2** **a** Pseudo-first-order kinetic and **b** pseudo-second-order kinetic models for adsorption process of **BUC-17** towards As(V) at 298 K

**Table 2** Kinetic parameters of pseudo-first-order and pseudo-second-order models for fitting kinetic data of As(V) adsorption with different concentration onto **BUC-17** (298 K)

| $C_0$ (mg $g^{-1}$) | Pseudo-first-order | | | Pseudo-second-order | | | Experimental value q (mg $g^{-1}$) |
|---|---|---|---|---|---|---|---|
| | $K_1$ ($min^{-1}$) | $q_e$ (mg $g^{-1}$) | $R^2$ | $K_2$ (g $mg^{-1}$ $min^{-1}$) | $q_e$ (mg $g^{-1}$) | $R^2$ | |
| 5 | 0.1169 | 18.87 | 0.9892 | 0.0136 | 24.99 | 0.9879 | 23.65 |
| 10 | 0.1466 | 29.35 | 0.9750 | 0.0131 | 45.35 | 0.9978 | 43.70 |
| 15 | 0.1885 | 32.11 | 0.8979 | 0.0145 | 58.55 | 0.9981 | 56.78 |
| 20 | 0.1794 | 33.58 | 0.9271 | 0.0166 | 74.57 | 0.9991 | 72.90 |
| 25 | 0.1742 | 28.28 | 0.8415 | 0.0153 | 82.51 | 0.9986 | 80.80 |
| 50 | 0.4623 | 92.56 | 0.9197 | 0.0131 | 116.82 | 0.9992 | 114.45 |
| 100 | 0.1290 | 41.64 | 0.6587 | 0.0145 | 131.41 | 0.9992 | 129.20 |

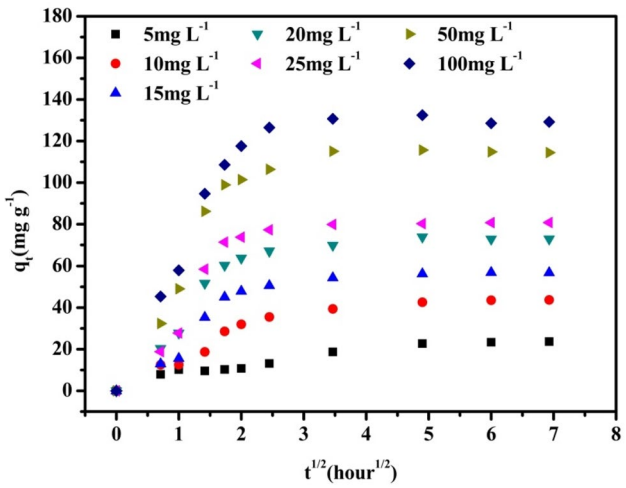


**Fig. 3** The Weber–Morris model for adsorption process of **BUC-17** towards As(V) at 298 K

## 3.2 Adsorption isotherms

To explore the relationship between temperature and adsorption capacity, series experiments were performed by adding 40 mg **BUC-17** samples to 200 mL As(V) solution with various initial concentrations (5–100 mg $L^{-1}$) at pH = 10. The suspensions were stirred at speed of 170 r $min^{-1}$ during the test in the shaker for 48 h to reach adsorption equilibrium at 298 K, 303 K and 308 K, respectively. The different isotherm models like Langmuir [47], Freundlich [48] and Dubinin–Radushkevich [49] (D-R) were adopted to explain the adsorption modes between adsorbent **BUC-17** and adsorbates As(V). The Langmuir, Freundlich and Dubinin–Radushkevich (D–R) isotherm models are demonstrated in Eqs. (5), (6) and (7), respectively.

$$C_e/q_e = 1/K_L q_{max} + C_e/q_{max} \quad (5)$$

$$\log q_e = \log K_f + (1/n)\log C_e \quad (6)$$

$$\ln q_e = \ln q_{max} - K_{DR}\xi^2 \quad (7)$$

where, $q_{max}$ (mg $g^{-1}$) is the theoretical maximum adsorption capacity toward As(V); $K_L$ is the Langmuir constant, which is related to adsorption energy; $q_e$ (mg $g^{-1}$) is the adsorption amount reaching adsorption equilibrium; $C_e$ (mg $L^{-1}$) is the equilibrium As(V) concentration; $K_f$ (mg $g^{-1}$) is the Freundlich constants, which indicates the adsorption ability of adsorbent; $n$ is a constant related

to system degree for adsorption; $K_{DR}$ (mol$^2$ J$^{-2}$) is the D–R constant related to average sorption energy; $\xi$ (J mol$^{-1}$) and E (kJ mol$^{-1}$) represents the Polanyi potential and adsorption free energy, respectively, which can be calculated by using Eqs. (8) and (9).

$$\xi = RT\ln\left(1 + 1/C_e\right) \tag{8}$$

$$E = 1/\left(2K_{DR}\right)^{1/2} \tag{9}$$

To clarify the adsorption mechanism of **BUC-17** toward As(V), the adsorption isotherms data were fitted with three isotherm models as shown in Fig. 4. The adsorption isotherm parameters are given in Table 3. It is clearly that the adsorption process was suitably fitted in Langmuir adsorption isotherm models with $R^2$ values over 0.99, which are well consistent with the adsorption process of **BUC-17** towards organic dyes [38] and Cr(VI) [39] as well as other adsorbents towards arsenic [7, 36], suggesting that the adsorption process is monolayer adsorption [43]. With the increase of temperature, the maximum adsorption capacity and Langmuir constant decreases continuously. Therefore, the adsorption process is an exothermic process, which was favorable at low temperature.

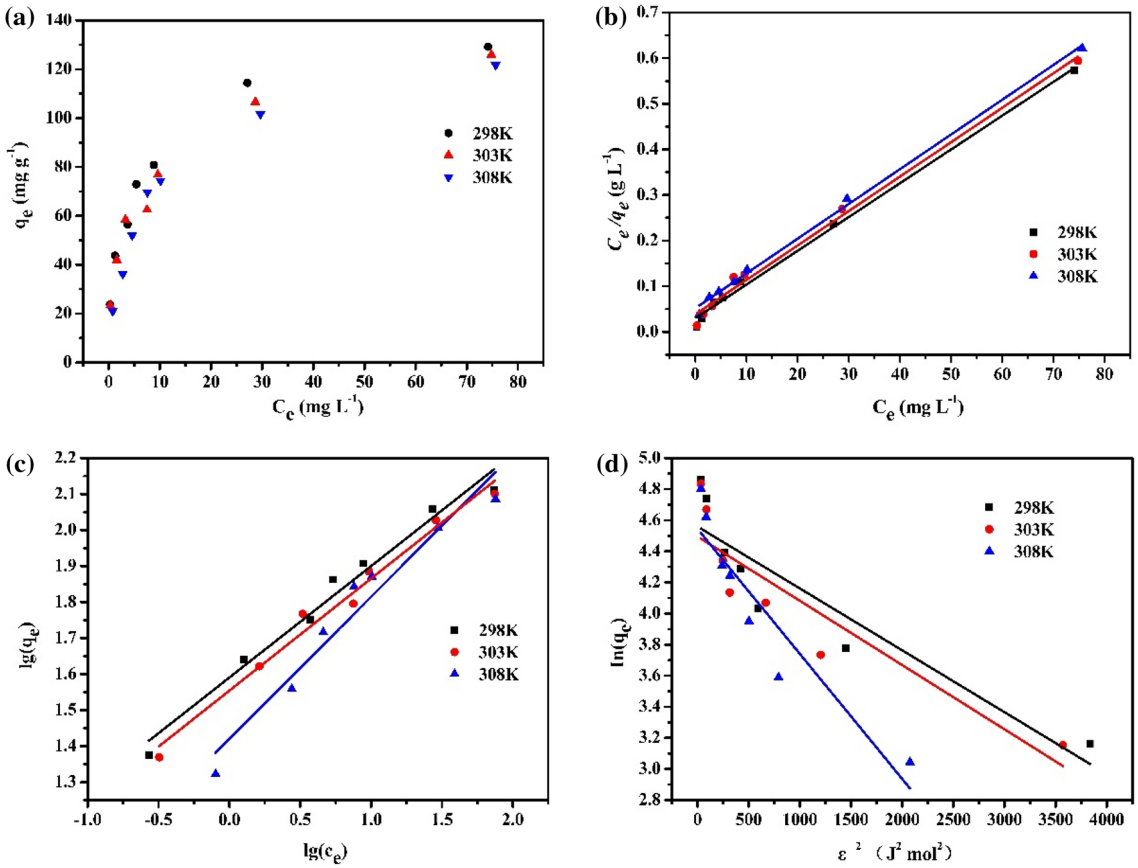


**Fig. 4** The **a** Equilibrium data for As(V) adsorption by **BUC-17** at different temperatures. **b** Langmuir, **c** Freundlich, and **d** Dubinin–Radushevich (D–R) adsorption isotherm models for adsorption of As(V) onto **BUC-17**

**Table 3** Constants of Langmuir, Freundich, and D–R for As(V) adsorption by **BUC-17** at different temperatures

| $T$(K) | Langmuir | | | Freundlich | | | D–R | | |
|---|---|---|---|---|---|---|---|---|---|
| | $K_L$(L mg$^{-1}$) | $q_m$ (mg g$^{-1}$) | $R^2$ | $K_f$ (L g$^{-1}$) | 1/$n$ | $R^2$ | $K_{DR}$ | $E$ (KJ mol$^{-1}$) | $R^2$ |
| 298 | 0.2515 | 134.96 | 0.9955 | 38.9466 | 0.3094 | 0.9727 | $3.98\times10^{-4}$ | 0.0251 | 0.8222 |
| 303 | 0.1983 | 132.45 | 0.9902 | 35.8162 | 0.3113 | 0.9772 | $4.13\times10^{-4}$ | 0.0246 | 0.7941 |
| 308 | 0.1473 | 131.23 | 0.9967 | 26.2839 | 0.3948 | 0.9415 | $8.04\times10^{-4}$ | 0.0176 | 0.8536 |

### 3.3 Thermodynamic calculations

The thermodynamic parameters which include standard Gibbs free energy ($\Delta G°$, kJ mol$^{-1}$), entropy change ($\Delta S°$, J mol$^{-1}$ K$^{-1}$) and enthalpy change ($\Delta H°$, kJ mol$^{-1}$) were calculated to get further insight into feasibility, favorability, and spontaneity of the adsorption process. They can be respectively calculated with the aid of data obtained from Langmuir adsorption isotherm via Eqs. (10) and (11) [50].

$$\Delta G° = -RT\ln K \tag{10}$$

$$\ln K = \Delta S°/R - \Delta H°/RT \tag{11}$$

where, $T$ (K) is the Kelvin temperature, $R$ (8.314 kJ mol$^{-1}$ K$^{-1}$) is the universal gas constant and $K$ is equilibrium coefficient estimated by the Langmuir parameter ($K_L$) [51] as Eq. (12):

$$K = K_L C_w \tag{12}$$

where, $C_w$ ($1.01 \times 10^6$ mg L$^{-1}$) represents the water concentration.

All the calculated thermodynamic parameters are illustrated in Table 4. In general, the free energy ($\Delta G°$) values ranging from − 20 to 0 kJ mol$^{-1}$ indicate that physi-sorption process predominates. While, $\Delta G°$ values between − 80 to − 400 kJ mol$^{-1}$ suggest chemisorption process [52]. In this study, the $\Delta G°$ values are − 30.84 kJ mol$^{-1}$, − 30.76 kJ mol$^{-1}$, − 30.50 kJ mol$^{-1}$ at 298 K, 303 K, 308 K, respectively, suggesting that physi-sorption process dominates in parallel with partial chemical sorption [52, 53]. Furthermore, the negative $\Delta G°$ values indicated that the adsorption process was a spontaneous process. The higher temperature led to declining adsorption capacity, which was confirmed by the maximum adsorption capacities of **BUC-17** decreasing from 134.96 mg g$^{-1}$ at 298 K to 131.23 mg g$^{-1}$ at 308 K. The value of $\Delta H°$ (−40.80 kJ mol$^{-1}$) suggests that the adsorption reaction is exothermic, while the negative of $\Delta S°$ value (− 33.22 J mol$^{-1}$ K$^{-1}$) implies that the randomness decreased after the adsorption process. All the thermodynamic parameters reveal that the adsorption processes are spontaneous and exothermic.

**Table 4** Thermodynamic parameters for As(V) adsorption via **BUC-17** at different temperatures

| $T$(K) | K | $\Delta G°$ (kJ mol$^{-1}$) | $\Delta S°$ (J mol$^{-1}$ K$^{-1}$) | $\Delta H°$ (kJ mol$^{-1}$) |
|---|---|---|---|---|
| 298 | 254,498 | − 30.84 | − 33.32 | − 40.80 |
| 303 | 200,664 | − 30.76 | | |
| 308 | 149,054 | − 30.50 | | |

### 3.4 Influencing factors

#### 3.4.1 Effect of pH

The pH value of As(V) solution is an extreme important factor to influence the adsorption process, because it determines the anionic species of arsenic along with the surface changes and the ionization of adsorbents [54, 55]. The effect of pH on the adsorption capacity was investigated in the pH range of 4.0–10.0, in which 40.0 mg **BUC-17** were added to 200 mL As(V) solution with initial concentration of 10 mg L$^{-1}$ under 298 K. As shown in Fig. 5a, the As(V) removal efficiency decrease dramatically from 10% at pH = 4.0 or 5.0 to 80% at pH = 10.0, which can be contributed to both the decreasing zeta potential of **BUC-17** and the different anionic species of As(V) in solution. The mainly anionic species of As(V) in solution under different pH values are $H_3AsO_4$ (pH < 2.3), $H_2AsO_4^-$ (3 < pH < 6), $HAsO_4^{2-}$ (8 < pH < 10.5), $AsO_4^{3-}$ (pH > 11) [56, 57]. With the increase of pH from 4.0 to 10.0, the average number of

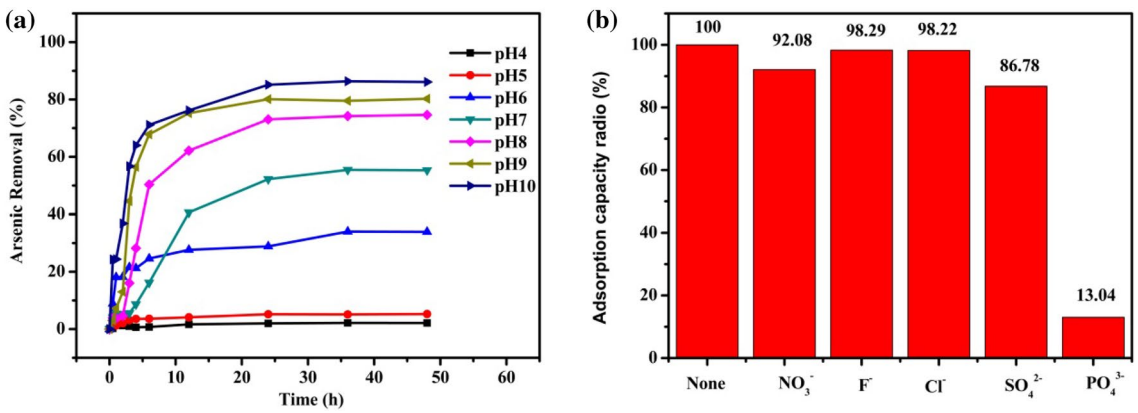


**Fig. 5** **a** The adsorption capacity of **BUC-17** toward As(V) under various pH values; **b** The adsorption capacity of **BUC-17** toward As(V) in the presence of different coexisting anions

negative charge of arsenate increases, which has positive effect on electrostatic attraction [57, 58]. Meanwhile, the zeta potential of **BUC-17** decreases from 4.0 to 10.0 [39], which leads to the gradually decreased area occupied by the average single arsenate adsorption, and exerts negative effect on electrostatic attraction. Finally, the combination of the two interactions leads to an enhancement of the adsorption capacity in total [43].

#### 3.4.2 Effect of coexisting anions

It is generally known that the co-existing anions in solution like nitrate, chlorate and phosphate are important factors in estimating its practical applicability as adsorbent [7]. To explore the effect of coexisting anions in As(V) solution, the experiment was demonstrated by adding 40 mg **BUC-17** into 200 mL solution containing 10 mg $L^{-1}$ of As(V) solution (pH = 10) with and without coexistent anions like $NO_3^-$, $F^-$, $Cl^-$, $SO_4^{2-}$, $PO_4^{3-}$ at 298 K. The concentration of all coexisting anions was 0.02 mol $L^{-1}$. The adsorption capacity ratio (%) are removal ratio without coexistent anions divide by removal ratio with coexistent anions. As shown in Fig. 5b, only 13.4% of the adsorption capacity was maintained in the presence of $PO_4^{3-}$, which may be due to phosphate and arsenate have similar adsorption behavior [59] and phosphate is more competitive for binding sites of **BUC-17** [37]. On the contrary, other co-existed anions like $NO_3^-$, $F^-$, $Cl^-$, $SO_4^{2-}$ exert no significant effect on adsorption capacity, which indicates that **BUC-17** displayed good adsorption efficiency in the presence of different anions unless phosphate.

### 3.5 Proposed adsorption mechanism

In order to confirm adsorption mechanism, the elemental mappings, FTIR spectra and XPS of **BUC-17** were obtained before and after As(V) adsorption. As shown in Fig. 6, the elemental mapping obtained from SEM verified the presence of As in **BUC-17** after adsorbing As(V) besides Co, O, N, S and C. What's more, the uptake of As(V) onto **BUC-17** can be also affirmed by FTIR spectra in Fig. 7b as a new adsorption band appeared at 881 $cm^{-1}$ which corresponds to the stretching vibration of As-O bond for **BUC-17** after adsorption [7, 60]. Furthermore, the main peaks of **BUC-17** before and after adsorption matched well in PXRD patterns as shown in Fig. 7a, the peaks of As(V)-loaded **BUC-17** were lower than the pristine **BUC-17**, as a result of the surface

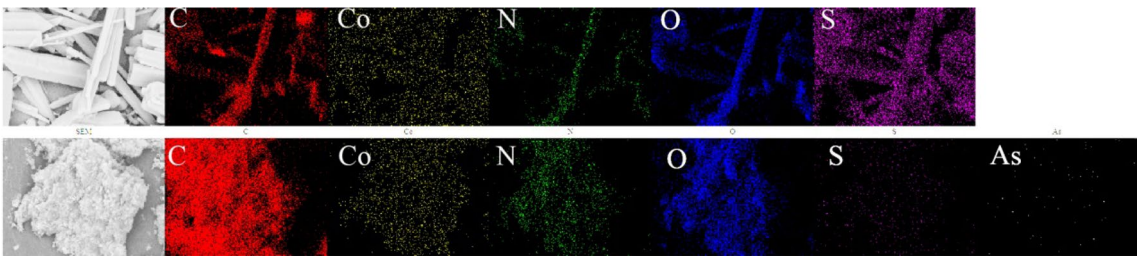


**Fig. 6** Elemental mapping of **BUC-17** before and after adsorption toward As(V)

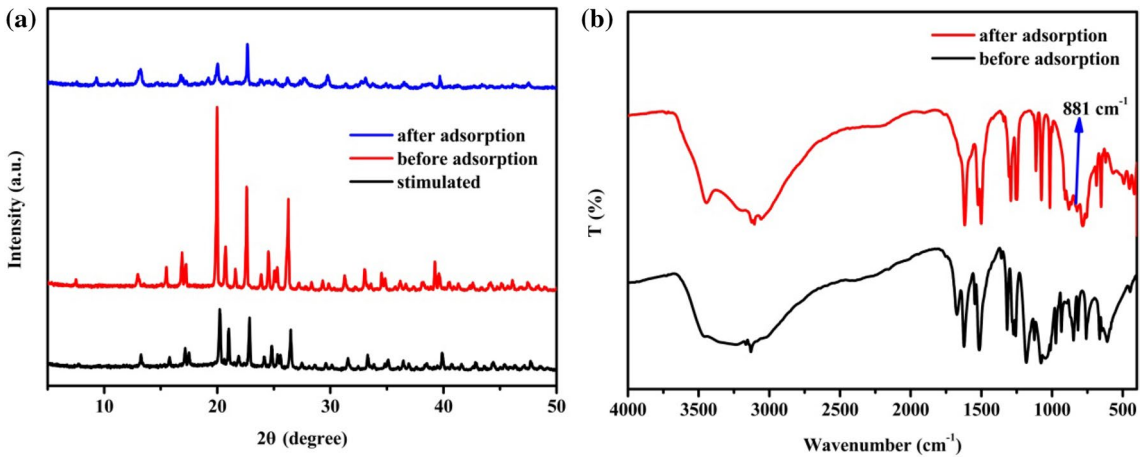


**Fig. 7** **a** The PXRD patterns of **BUC-17** before and after adsorption toward As(V); **b** The FTIR spectra of **BUC-17** before and after adsorption toward As(V)

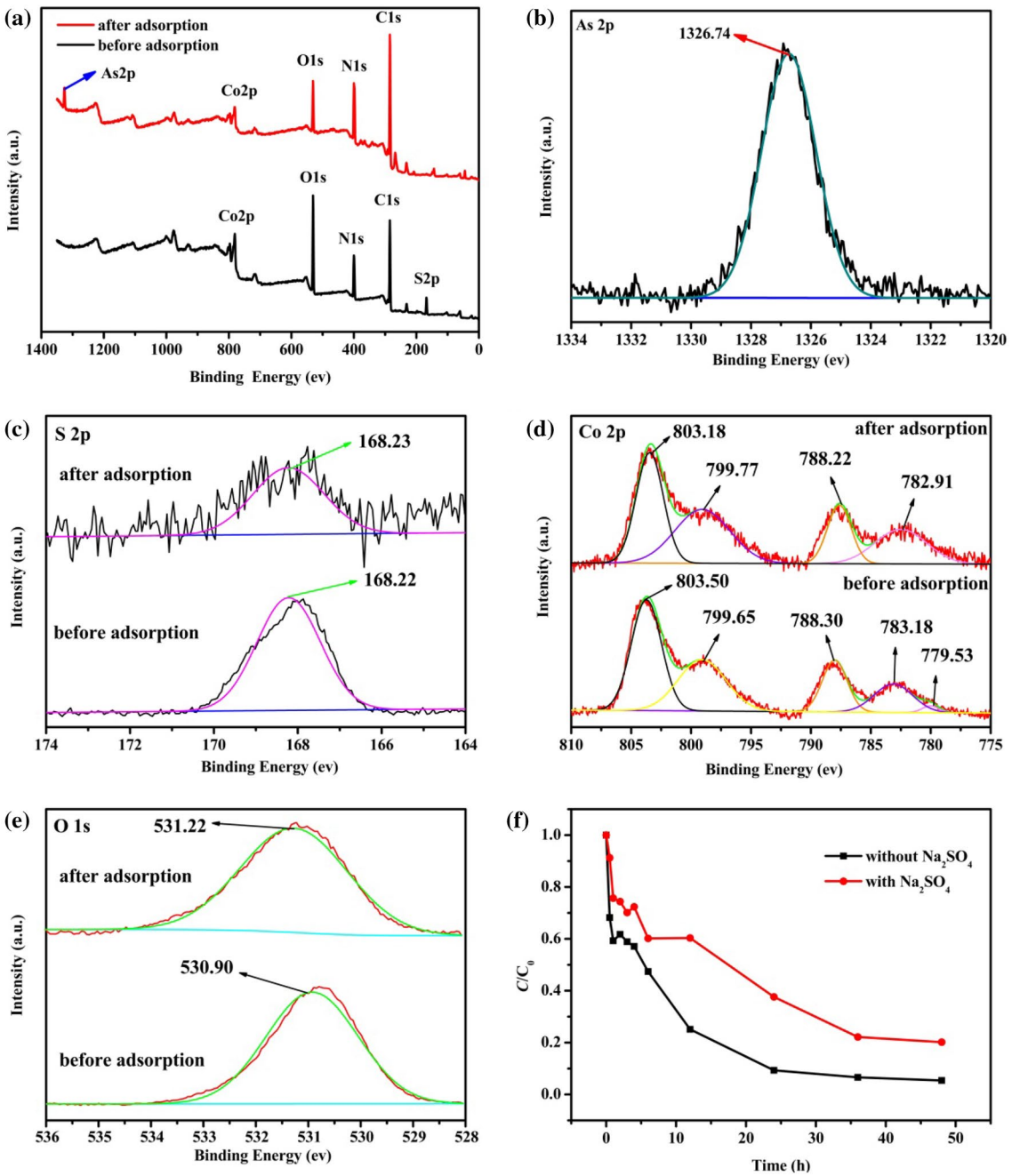


**Fig. 8** **a** Full range XPS spectra of **BUC-17** before and after As(V) adsorption; **b** XPS spectra of As 2p before and after As(V) adsorption; **c** XPS spectra of S 2p before and after As(V) adsorption; **d** XPS spectra of Co 2p before and after As(V) adsorption; **e** XPS spectra of O 1 s before and after As(V) adsorption; **f** Adsorption of As(V) in deionized water and in saturated $Na_2SO_4$ solution with **BUC-17**

of **BUC-17** covered with the adsorbed As(V), which affirmed a good stability of **BUC-17** during the adsorption process [36].

The BET surface area of **BUC-17** is 2.39 $m^2\ g^{-1}$ and the pore size of **BUC-17** is ca. 2.36 nm [38], indicating that its highly efficient adsorption towards arsenate might not be attributed to its porosity. As previously reported by Li et al. and Guo et al., **BUC-17** has an overall positive surface charge from pH = 4 to pH = 10 [38, 39], demonstrating that electrostatic interaction contributed to the adsorption

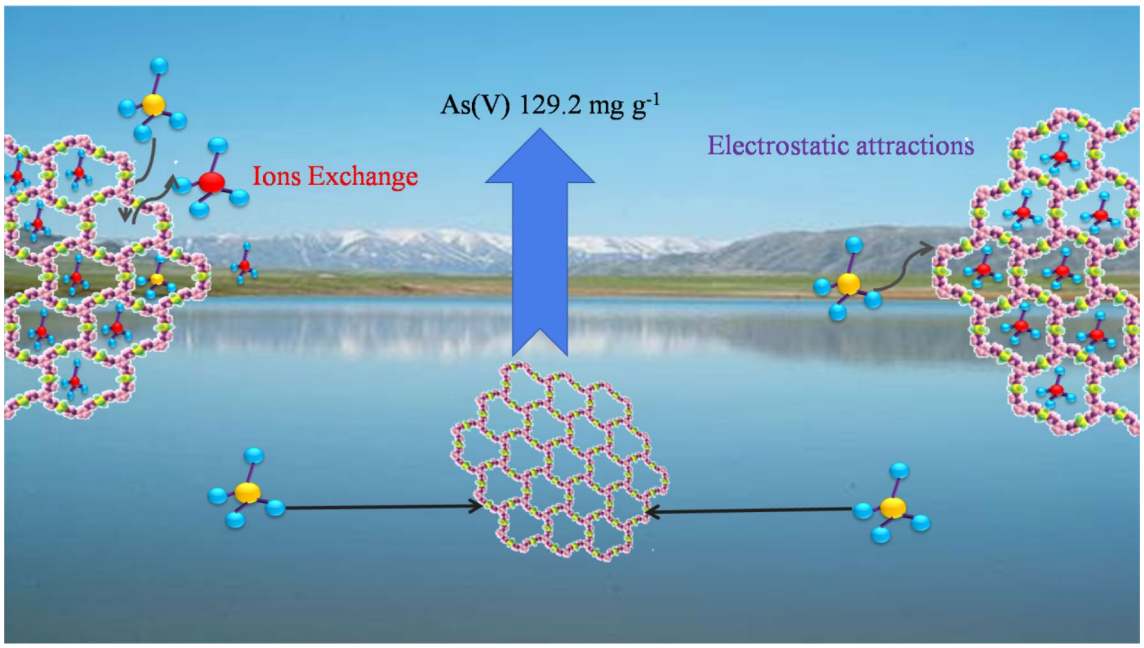


**Fig. 9** Proposed interaction mechanism between As(V) and **BUC-17**

process of As(V) by **BUC-17**. In addition, the decrease of S element accompanied with the increase As element after adsorption were obtained from SEM indicated that ion-exchange interactions exist in the adsorption process. The experiment was conducted to study adsorption capacity towards As(V) in saturated aqueous $Na_2SO_4$ solution and in pure aqueous solution. As illustrated in Fig. 8f, the presence of $SO_4^{2-}$ obviously inhibited the As(V) adsorption onto **BUC-17**, as confirmed by the removal efficiency decrease from 94.6% (without $Na_2SO_4$ aqueous solution) to 79.8% (saturated $Na_2SO_4$ aqueous solution) with initial solution concentration of 5 mg $L^{-1}$. What's more, the decrease of the uncoordinated $SO_4^{2-}$ from **BUC-17** was evidenced by XPS, in which the binding energy of 168.22 eV (S 2p) belonging to $SO_4^{2-}$ decreased sharply. Meanwhile, a new As 2p (1326.74 eV) peaks of arsenate emerged after adsorption, suggesting that ion-exchange interactions played an important role in the adsorption process [61, 62]. Therefore, the possible adsorption mechanism of As(V) onto **BUC-17** were ion-exchange interactions and electrostatic interaction as illustrated in Fig. 9.

## 4 Conclusion

In this study, **BUC-17** exhibited good adsorption performance for the As(V) removal from wastewater; the adsorption kinetics and adsorption isotherm of As(V) on **BUC-17** were suitably fitted by the pseudo-second-order kinetic model, and Langmuir isotherm model, respectively, and the maximum adsorption capacity was 129.2 mg $g^{-1}$, higher than most reported adsorbents for As(V) removal. The adsorption process was spontaneous, exothermic and the randomness decreased as the result of negative ΔG°, ΔH° and ΔS° values. The pH values and foreign ions were also important influence factors during the whole adsorption process. The possible adsorption mechanisms in this study were proposed, including electrostatic and ion-exchange interactions. With the good adsorption performance towards As(V), **BUC-17** could be potentially applied in industrial wastewater treatment.

**Funding** The authors acknowledge financial support from Project of the National Science Foundation of China (51878023,51578034), Construction of Innovation Teams and Teacher Career Development for Universities and Colleges Under Beijing Municipality (IDHT20170508), Great Wall Scholars Training Program Project of Beijing Municipality Universities (CIT&TCD20180323), Beijing Talent Project (2019A22), the Fundamental Research Funds for Beijing Universities of Civil Engineering and Architecture (X18276) and Scientific Research Foundation of Beijing University of Civil Engineering and Architecture (KYJJ2017008).

### Compliance with ethical standards

**Conflict of interest** The authors declare that they have no conflict of interest.

## References


1. Hughes MF et al (2011) Arsenic exposure and toxicology: a historical perspective. Toxicol Sci 123(2):305–332
2. Song P et al (2017) Electrocoagulation treatment of arsenic in wastewaters: a comprehensive review. Chem Eng J 317:707–725
3. Choong TSY et al (2007) Arsenic toxicity, health hazards and removal techniques from water: an overview. Desalination 217(1–3):139–166
4. Mandal BK, Suzuki KT (2002) Arsenic round the world: a review. Talanta 58(1):201–235
5. Jain CK, Ali I (2000) Arsenic: occurrence, toxicity and speciation techniques. Water Res 34(17):4304–4312
6. Carlin DJ et al (2016) Arsenic and environmental health: state of the science and future research opportunities. Environ Health Perspect 124(7):890–899
7. Yu W et al (2019) Metal–organic framework (MOF) showing both ultrahigh As(V) and As(III) removal from aqueous solution. J Solid State Chem 269:264–270
8. Smedley PL, Kinniburgh DG (2002) A review of the source, behaviour and distribution of arsenic in natural waters. Appl Geochem 17(5):517–568
9. Nrashant S, Deepak K, Anand PS (2007) Arsenic in the environment : effects on human health and possible prevention. J Theor Biol 28(2):359–365
10. Kapaj S et al (2006) Human health effects from chronic arsenic poisoning–a review. J Environ Sci Health A Tox Hazard Subst Environ Eng 41(10):2399–2428
11. Nicomel NR et al (2015) Technologies for arsenic removal from water: current status and future perspectives. Int J Environ Res Public Health 13(1):62
12. Wu H et al (2018) Arsenic removal from water by metal–organic framework MIL-88A microrods. Environ Sci Pollut Res Int 25(27):27196–27202
13. Zhang X et al (2017) Simultaneous oxidation and sequestration of As(III) from water by using redox polymer-based Fe(III) oxide nanocomposite. Environ Sci Technol 51(11):6326–6334
14. Li H et al (2016) Long-term performance of rapid oxidation of arsenite in simulated groundwater using a population of arsenite-oxidizing microorganisms in a bioreactor. Water Res 101(15):393–401
15. Gill LW, O'Farrell C (2015) Solar oxidation and removal of arsenic–Key parameters for continuous flow applications. Water Res 86(1):46–57
16. Vahter M (2002) Mechanisms of arsenic biotransformation. Toxicology 181(181–182):211–217
17. Federico B et al (1987) Cellular uptake and metabolic reduction of pentavalent to trivalent arsenic as determinants of cytotoxicity and morphological transformation. Carcinogenesis 8(6):803–808
18. Li J et al (2014) Characteristics of arsenate removal from water by metal-organic frameworks (MOFs). Water Sci Technol 70(8):1391–1397
19. Bissen M, Frimmel FH (2003) Arsenic—a review. Part II: oxidation of arsenic and its removal in water treatment. Acta Hydroch Hydrob 31(2):97–107
20. Simsek EB, Özdemir E, Beker U (2013) Zeolite supported mono- and bimetallic oxides: promising adsorbents for removal of As(V) in aqueous solutions. Chem Eng J 220(11):402–411
21. Gupta SK, Chen KY (1978) Arsenic removal by adsorption. Water Pollut Contr Fed 50(3):493–506
22. Clifford DA, Ghurye G, Tripp AR (2003) Arsenic removal from drinking Water using ion-exchange with spent brinere cycling. J Am Water Works Ass 95(6):119–130
23. Ng KS, Ujang Z, Le.Clech P (2004) Arsenic removal technologies for drinking water treatment. Rev Environ Sci Biotechnol 3(1):43–53
24. Huang CP, Fu PLK (1984) Treatment of Arsenic(V)-containing water by the activated carbon process. Water Pollut Contr Fed 56(3):233–242
25. Gillman GP (2006) A simple technology for arsenic removal from drinking water using hydrotalcite. Sci Total Environ 366(2–3):926–931
26. Altundogan H, Fikret F (2003) As(V) removal from aqueous solutions by coagulation with liquid phase of red mud. J Environ Sci Health Part A 38(7):1247–1258
27. Lin TF, Wu JK (2001) Adsorption of arsenite and arsenate within activated alumina grains equilibrium and kinetics. Water Res 35(8):2049–2057
28. Wang C-C et al (2014) Photocatalytic organic pollutants degradation in metal–organic frameworks. Energy Environ Sci 7(9):2831–2867
29. Wang C-C, Yi X-H, Wang P (2019) Powerful combination of MOFs and $C_3N_4$ for enhanced photocatalytic performance. Appl Catal B 247:24–48
30. Du X-D et al (2019) Robust photocatalytic reduction of Cr(VI) on UiO-66-$NH_2$(Zr/Hf) metal–organic framework membrane under sunlight irradiation. Chem Eng J 356:393–399
31. Fu H-F et al (2018) Formation mechanism of rod-like ZIF-L and fast phase transformation from ZIF-L to ZIF-8 with morphology changes controlled by polyvinylpyrrolidone and ethanol. Cryst Eng Comm 20(11):1473–1477
32. Yi X-H et al (2018) Highly efficient photocatalytic Cr(VI) reduction and organic pollutants degradation of two new bifunctional 2D Cd/Co-based MOFs. Polyhedron 152:216–224
33. Xie D et al (2017) Bifunctional $NH_2$-MIL-88(Fe) metal–organic framework nanooctahedra for highly sensitive detection and efficient removal of arsenate in aqueous media. J Mater Chem A 5(45):23794–23804
34. He X et al (2019) Exceptional adsorption of arsenic by zirconium metal-organic frameworks: engineering exploration and mechanism insight. J Colloid Interface Sci 539:223–234
35. Tian C et al (2018) Enhanced adsorption of p-Arsanilic acid from Water by amine-modified UiO-67 as examined using extended X-ray absorption fine structure, x-ray photoelectron spectroscopy, and density functional theory calculations. Environ Sci Technol 52(6):3466–3475
36. Jian M et al (2015) Adsorptive removal of arsenic from aqueous solution by zeolitic imidazolate framework-8 (ZIF-8) nanoparticles. Colloid Surface A 465:67–76
37. Li J et al (2014) Zeolitic Imidazolate framework-8 with high efficiency in trace arsenate adsorption and removal from water. J Phys Chem C 118(47):27382–27387
38. Li J-J et al (2017) High-performance adsorption and separation of anionic dyes in water using a chemically stable graphene-like metal-organic framework. Dalton Trans 46(31):10197–10201
39. Guo J, Li J-J, Wang C-C (2019) Adsorptive removal of Cr(VI) from simulated wastewater in MOF BUC-17 ultrafine powder. J Environ Chem Eng 7(1):102909
40. Ofomaja AE, Naidoo EB, Modise SJ (2010) Kinetic and pseudo-second-order modeling of lead biosorption onto pine cone powder. Ind Eng Chem Res 49(6):2562–2572
41. Wu YN et al (2014) Amino acid assisted templating synthesis of hierarchical zeolitic imidazolate framework-8 for efficient arsenate removal. Nanoscale 6(2):1105–1112
42. Vu TA et al (2015) Arsenic removal from aqueous solutions by adsorption using novel MIL-53(Fe) as a highly efficient adsorbent. RSC Adv 5(7):5261–5268

43. Abu Tarboush BJ et al (2018) Metal–organic framework-74 for ultratrace arsenic removal from water: experimental and density functional theory studies. ACS Appl Nano Mater 1(7):3283–3292
44. Li Z-Q et al (2015) Facile synthesis of metal–organic framework MOF-808 for arsenic removal. Mater Lett 160:412–414
45. Yang JC, Yin XB (2017) $CoFe_2O_4$@MIL-100(Fe) hybrid magnetic nanoparticles exhibit fast and selective adsorption of arsenic with high adsorption capacity. Sci Rep 7:40955
46. Faria MCS et al (2014) Arsenic removal from contaminated water by ultrafine δ-FeOOH adsorbents. Chem Eng J 237:47–54
47. Zhao X, Jia Q, Song N (2010) Adsorption of Pb(II) from an aqueous solution by titanium dioxide/carbon nanotube nanocomposites: kinetics, thermodynamics, and isotherms†. J Chem Eng Data 55(10):4428–4433
48. Kumar M, Tamilarasan R, Sivakumar V (2013) Adsorption of Victoria blue by carbon/Ba/alginate beads: kinetics, thermodynamics and isotherm studies. Carbohydr Polym 98(1):505–513
49. Eren E (2009) Removal of basic dye by modified Unye bentonite. Turkey. J Hazard Mater 162(2–3):1355–1363
50. Bulut Y, Tez Z (2007) Adsorption studies on ground shells of hazelnut and almond. J Hazard Mater 149(1):35–41
51. Milonjic SK (2007) A consideration of the correct calculation of thermodynamic parameters of adsorption. Serb Chem Soc 72(12):1363–1367
52. Zaki AB et al (2000) Kinetics and mechanism of the sorption of some aromatic amines onto amberlite IRA-904 anion-exchange resin. J Colloid Interface Sci 221(1):58–63
53. Du X-D et al (2017) Highly efficient removal of $Pb^{2+}$ by a polyoxomolybdate-based organic–inorganic hybrid material {$(4\text{-Hap})_4[Mo_8O_{26}]$}. J Environ Chem Eng 5(2):1866–1873
54. Lu P, Zhu C (2010) Arsenic Eh–pH diagrams at 25 °C and 1 bar. Environ Earth Sci 62(8):1673–1683
55. Heibati B et al (2016) Removal of linear alkyl benzene sulfonate from aqueous solutions by functionalized multi-walled carbon nanotubes. J Mol Liq 213:339–344
56. Cumbal L, SenGupta AK (2005) Arsenic removal using polymer-supported hydrated iron(III) oxide nanoparticles: role of Donnan membrane effect. Environ Sci Technol 39(17):6508–6515
57. Chen B et al (2013) Facile synthesis of mesoporous Ce–Fe bimetal oxide and its enhanced adsorption of arsenate from aqueous solutions. J Colloid Interface Sci 398:142–151
58. Sharma VK, Sohn M (2009) Aquatic arsenic: toxicity, speciation, transformations, and remediation. Environ Int 35(4):743–759
59. Amita J, Richard HL (2000) Effect of competing anions on the adsorption of arsenate and arsenite by ferrihydrite. J Environ Qual 29(5):1422–1430
60. Castaldi P et al (2010) Study of sorption processes and FT-IR analysis of arsenate sorbed onto red muds (a bauxite ore processing waste). J Hazard Mater 175(1–3):172–178
61. Song X-X et al (2018) The selectively fluorescent sensing detection and adsorptive removal of $Pb^{(2+)}$ with a stable [delta-$Mo_8O_{26}$]-based hybrid. J Colloid Interface Sci 532:598–604
62. Tan X-L et al (2009) Eu(III) sorption to $TiO_2$ (anatase and rutile): batch, XPS, and EXAFS studies. Environ Sci Technol 43(9):3115–3121